nature nanotechnology

ARTICLES

PUBLISHED ONLINE: 15 DECEMBER 2013 | DOI: 10.1038/NNANO.2013.267

Spin-resolved Andreev levels and parity crossings in hybrid superconductor–semiconductor nanostructures

Eduardo J. H. Lee[1], Xiaocheng Jiang[2], Manuel Houzet[1], Ramón Aguado[3], Charles M. Lieber[2] and Silvano De Franceschi[1]*

The physics and operating principles of hybrid superconductor–semiconductor devices rest ultimately on the magnetic properties of their elementary subgap excitations, usually called Andreev levels. Here we report a direct measurement of the Zeeman effect on the Andreev levels of a semiconductor quantum dot with large electron *g*-factor, strongly coupled to a conventional superconductor with a large critical magnetic field. This material combination allows spin degeneracy to be lifted without destroying superconductivity. We show that a spin-split Andreev level crossing the Fermi energy results in a quantum phase transition to a spin-polarized state, which implies a change in the fermionic parity of the system. This crossing manifests itself as a zero-bias conductance anomaly at finite magnetic field with properties that resemble those expected for Majorana modes in a topological superconductor. Although this resemblance is understood without evoking topological superconductivity, the observed parity transitions could be regarded as precursors of Majorana modes in the long-wire limit.

When a normal-type (N) conductor is connected to a superconductor (S), superconducting order can leak into it to give rise to pairing correlations and an induced superconducting gap. This phenomenon, known as the superconducting proximity effect, is also expected when the N conductor consists of a nanoscale semiconductor whose electronic states have a reduced dimensionality and can be tuned by means of electric or magnetic fields. This hybrid combination of superconductors and low-dimensional semiconductors offers a versatile ground for novel device concepts[1]. Some examples include sources of spin-entangled electrons[2–4], nanoscale superconducting magnetometers[5] or recently proposed qubits based on topologically protected Majorana fermions[6–8]. Such concepts, which form an emerging domain between superconducting electronics and spintronics, rest on a rich and largely unexplored physics that involves both superconductivity and spin-related effects[5,9–12]. Here we address this subject by considering the lowest dimensional limit where the N conductor behaves as a small quantum dot (QD) with a discrete electronic spectrum. In this case, the superconducting proximity effect competes with the Coulomb blockade phenomenon, which follows from the electrostatic repulsion among the electrons of the QD[13]. Although superconductivity privileges the tunnelling of Cooper pairs of electrons with opposite spin, and thereby favours QD states with even numbers of electrons and zero total spin (that is, spin singlets), the local Coulomb repulsion enforces a one-by-one filling of the QD, and thereby stabilizes not only even but also odd electron numbers.

To analyse this competition, let us consider the elementary case of a QD with a single, spin-degenerate orbital level. When the dot occupation is tuned to one electron, two ground states (GSs) are possible: a spin doublet (spin 1/2), $|D\rangle = |\uparrow\rangle, |\downarrow\rangle$, or a spin singlet (spin zero), $|S\rangle$, whose nature has two limiting cases. In the large superconducting gap limit ($\Delta \to \infty$), the singlet is superconducting like, $|S\rangle = -v^*|\uparrow\downarrow\rangle + u|0\rangle$, which corresponds to a Bogoliubov-type superposition of the empty state, $|0\rangle$, and the two-electron state, $|\uparrow\downarrow\rangle$. By contrast, in the strong coupling limit, where the QD–S tunnel coupling, Γ_S, is much larger than Δ, the singlet state is Kondo-like, resulting from the screening of the local QD magnetic moment by quasiparticles in S. Even though the precise boundary between the superconducting-like and Kondo-like singlet states is not well-defined[14], one can clearly identify changes in the GS parity, namely whether the GS is a singlet (fermionic even parity) or a doublet (fermionic odd parity), as we show here. The competition between the singlet and doublet states is governed by different energy scales: Δ, Γ_S, the charging energy, U, and the energy, ε_0, of the QD level relative to the Fermi energy of the S electrode (see Fig. 1a)[14–23]. Previous works that address this competition focused either on Josephson supercurrents in S–QD–S devices[11,24] or on the subgap structure in S–QD–S or N–QD–S geometries[25–33]. Although the QD–S GS could be inferred in some of the above studies, a true experimental demonstration of the GS parity requires its magnetic properties to be probed.

Here we report a tunnel spectroscopy experiment that probes the magnetic properties of a QD–S system. With the aid of suitably large magnetic fields, we lifted the degeneracy of the spinful states (that is, $|D\rangle$) and measured the corresponding effect on the lowest-energy subgap excitations of the system (that is, $|D\rangle \leftrightarrow |S\rangle$ transitions). This experiment was carried out on a N–QD–S system, where the N contact is used as a weakly coupled tunnel probe. In this geometry, a direct spectroscopy of the density of states in the QD–S system is obtained through a measurement of the differential conductance, dI/dV, as a function of the voltage difference, V, between N and S. In such a measurement, an electrical current measured for $|V| < \Delta/e$ is carried by so-called Andreev reflection processes, each of which

[1]SPSMS, CEA-INAC/UJF-Grenoble 1, 17 rue des Martyrs, 38054 Grenoble Cedex 9, France, [2]Harvard University, Department of Chemistry and Chemical Biology, Cambridge, Massachusetts 02138, USA, [3]Instituto de Ciencia de Materiales de Madrid, Consejo Superior de Investigaciones Científicas (CSIC), Sor Juana Inés de la Cruz 3, 28049 Madrid, Spain. *e-mail: silvano.defranceschi@cea.fr

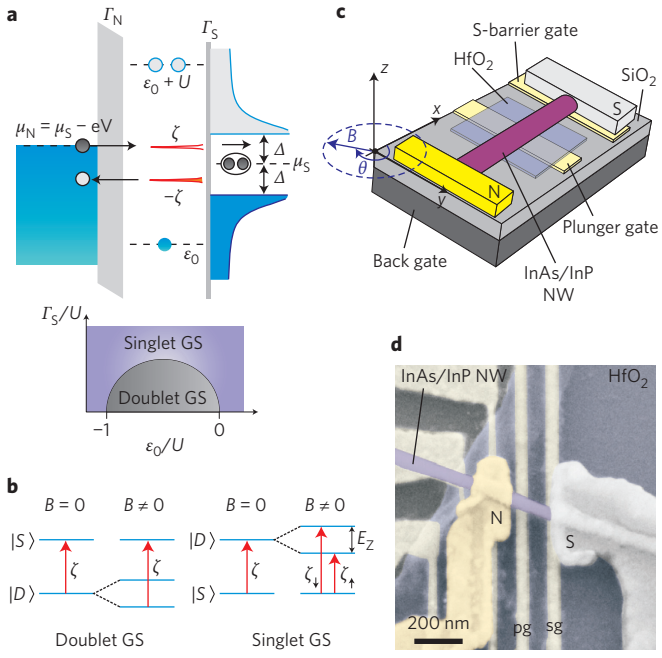

Figure 1 | Andreev levels in a hybrid N–QD–S system and device description. a, The upper panel shows schematics of a N–QD–S device with asymmetric tunnel couplings to the normal metal (Au) and superconductor (V) leads, Γ_N and Γ_S, respectively. Δ is the superconducting gap, U is the charging energy, μ_i is the chemical potential of the i lead and ε_0 is the QD energy level relative to μ_S (in the $\Gamma_S \to 0$ limit, the QD has zero, one or two electrons for $\varepsilon_0 > 0$, $-U < \varepsilon_0 < 0$ or $\varepsilon_0 < -U$, respectively). The subgap peaks located at $\pm\zeta$ represent the Andreev levels. In tunnel spectroscopy measurements the alignment of μ_N to an Andreev level yields a peak in the differential conductance. This process involves an Andreev reflection at the QD–S interface, which transports a Cooper pair to the S lead and reflects a hole to the N contact. The qualitative phase diagram[16–19,21] (lower panel) depicts the stability of the magnetic doublet ($|D\rangle = |\uparrow\rangle, |\downarrow\rangle$) versus that of the spin singlet ($|S\rangle$). **b**, Low-energy excitations of the QD–S system and their expected evolution in a magnetic field, B. Doublet GS case (left): $|\uparrow\rangle$ is stabilized by B and Andreev levels related to the transition $|\uparrow\rangle \to |S\rangle$ are observed. Singlet GS case (right): at finite B, the excited spin-split states $|\uparrow\rangle$ and $|\downarrow\rangle$ give rise to distinct Andreev levels with energy $\zeta_\uparrow$ and $\zeta_\downarrow$, respectively. $E_Z = |g|\mu_B B$ is the Zeeman energy, where $|g|$ is the g-factor and μ_B is the Bohr magneton. **c**, Device schematic: the N and S leads were made of Ti (2.5 nm)/Au (50 nm) and Ti (2.5 nm)/V (45 nm)/Al (5 nm), respectively. The QD system is tuned by means of three gates: a plunger gate, a barrier gate close to the S contact and a back gate. B is applied in the (x, y) device plane (x being parallel to the NW). **d**, Scanning electron micrograph of a N–QD–S device.

involves two single-electron transitions in the QD. For example, an electron entering the QD from N induces a single-electron transition from the QD GS, that is $|D\rangle$ or $|S\rangle$, to the first excited state (ES), that is $|S\rangle$ or $|D\rangle$, respectively. The ES relaxes back to the GS through the emission of an electron pair into the superconducting condensate of S and a second single-electron transition, which corresponds to the injection of another electron from N (the latter process is usually seen as the retroreflection of a hole into the Fermi sea of N). The just-described transport cycle yields a dI/dV resonance, that is an Andreev level, at $eV = \zeta$, where ζ is the energy difference between ES and the GS, that is between $|D\rangle$ or $|S\rangle$, or vice versa (see Fig. 1a). The reverse cycle, which involves the same excitations, occurs at $eV = -\zeta$ to yield a second Andreev level symmetrically positioned below the Fermi level.

In a magnetic field, the spin doublet splits because of the Zeeman effect. Remarkably, as Andreev levels are associated with low-energy transitions between states with different parity, a corresponding splitting of the Andreev levels is expected only for a spin-singlet GS (Fig. 1b, right). In the case of a spin-doublet GS, the spin-flip transition does not generate any measurable subgap resonance, and the Zeeman splitting of $|D\rangle$ results simply in an increase of ζ (Fig. 1b, left). The main goal of this work is to reveal the Zeeman effect on the Andreev levels of a QD–S system and to investigate its experimental signatures as a function of the relevant energy scales and the corresponding GS properties.

We used devices based on single InAs/InP core/shell nanowires (NWs), where vanadium (gold) was used for the S (N) contact[34]. A device schematic and a representative image are shown in Figs 1c,d, respectively. The fabricated vanadium electrodes showed $\Delta = 0.55$ meV and an in-plane critical magnetic field $B_c^x \approx 2$ T ($x \parallel$ NW axis). The QD is naturally formed in the NW section between the S and N contacts. We found typical U values of a few millielectronvolts (that is, $U/\Delta \approx 3$–10). The QD properties are controlled by means of two bottom electrodes that cross the NW, labelled as plunger gate and S-barrier gate, and a back gate provided by the conducting Si substrate. To achieve the asymmetry condition $\Gamma_S \gg \Gamma_N$ ($\Gamma_S/\Gamma_N \approx 100$), the S-barrier gate was positively biased at $V_{sg} = 2$ V. We used the plunger-gate voltage, V_{pg}, to vary the charge on the QD, and the back-gate voltage, V_{bg}, to tune the tunnel coupling finely. Transport measurements were performed in a dilution refrigerator with a base temperature of 15 mK.

Figure 2 shows a series of $dI/dV(V_{pg},V)$ measurements for three different Γ_S. The top row refers to the weakest Γ_S. In this case, the spanned V_{pg} range corresponds to a horizontal path in the phase diagram that goes through the doublet GS region (schematic on the right-hand side of the top row). Let us first consider the left-most plot taken at magnetic field $B = 0$. On the left and right sides of this plot, the QD lies deep inside the singlet GS regime. Here the doublet ES approaches the superconducting gap edge to yield an Andreev-level energy $\zeta \approx \Delta$. By moving towards the central region, the two subgap resonances approach each other and cross at the singlet–doublet phase boundaries, where $\zeta = 0$. In the doublet GS regime between the two crossings, the subgap resonances form a loop structure with ζ maximal at the electron-hole symmetry point. Increasing Γ_S corresponds to an upwards shift in the phase diagram. The middle row in Fig. 2 refers to the case where Γ_S is just large enough to stabilize the singlet GS over the full V_{pg} range (schematic on the right-hand side of the middle row). At $B = 0$, the Andreev levels approach the Fermi level without crossing it. A further increase in Γ_S leads to a robust stabilization of the singlet GS (bottom row). This corresponds to a horizontal path well above the doublet GS region (schematic on the right-hand side of the bottom row). At zero field, the subgap resonances remain distant from each other, coming to a minimal separation at the electron-hole symmetry point ($\varepsilon_0 = -U/2$).

We now turn to the effect of B on the Andreev levels (second and third columns in Fig. 2, B along x). Starting from the weak coupling case (top row), a field-induced splitting of the subgap resonances appears, yet only in correspondence with a singlet GS. This is because these resonances involve excitations between states of different parity. For a singlet GS, the spin degeneracy of the doublet ES is lifted by the Zeeman effect, which results in two distinct excitations (see Fig. 1b). By contrast, for a doublet GS, no subgap resonance stems from the $|\uparrow\rangle \to |\downarrow\rangle$ excitation, because these two states have the same (odd) number of electrons. The energy of the only visible Andreev level associated with the $|\uparrow\rangle \to |S\rangle$ transition increases with B. The formation of a loop structure in the third panel of the middle row shows that a quantum phase transition (QPT) from a singlet to a spin-polarized GS can be induced by B when the starting ζ is sufficiently small. Importantly, this QPT is indicative of a change in the fermion parity of the GS. In the

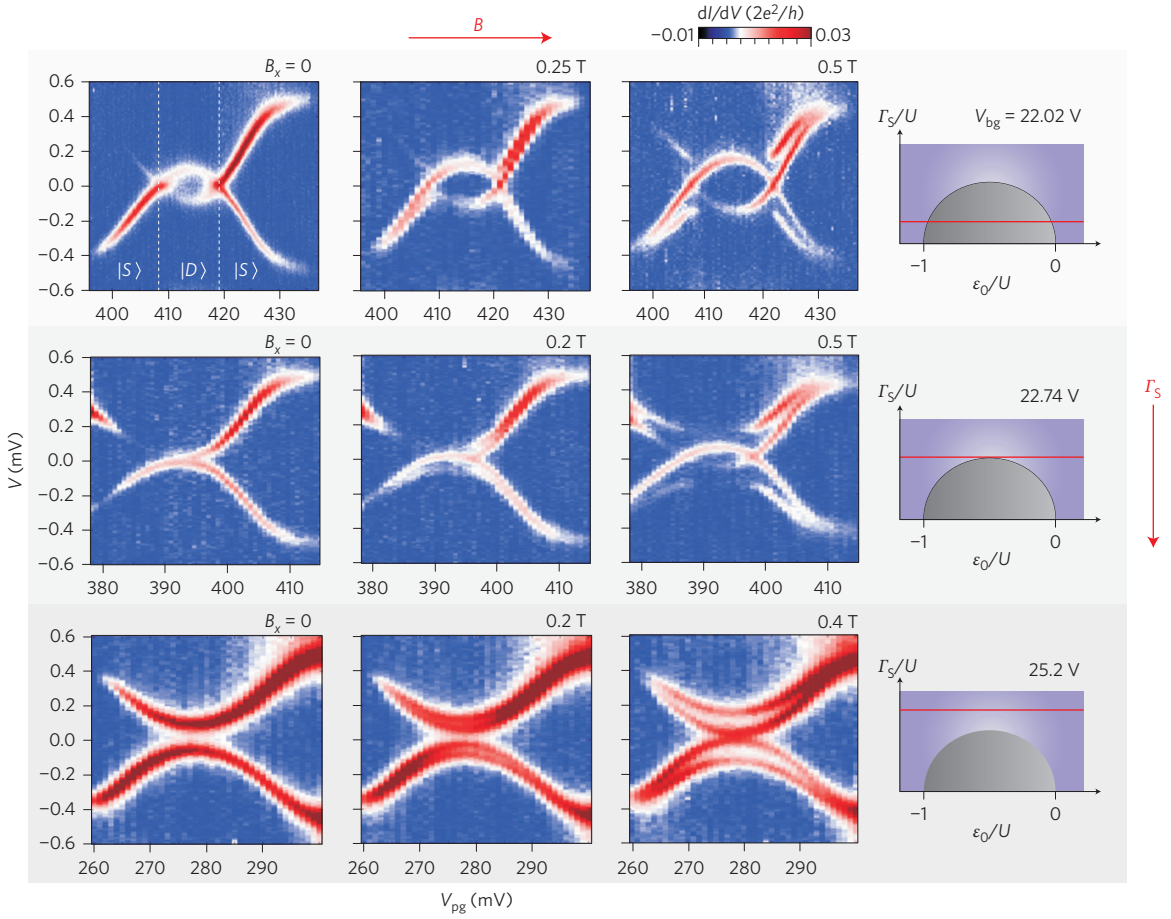

Figure 2 | Andreev levels in different coupling regimes and their magnetic-field dependence. Experimental plots of d*I*/d*V* versus (V_{pg},*V*) for different QD–S couplings, Γ_S (increasing from top to bottom) and magnetic fields parallel to the NW axis (B_x increasing from left to right). Along the V_{pg} range of the top-left panel, the system GS changes from singlet (|*S*⟩) to doublet (|*D*⟩) and back to singlet, following the red trajectory in the qualitative diagram on the right side of the same row. We found that increasing V_{bg} resulted in larger Γ_S, which thereby leads to an upwards shift in the phase diagram. Eventually, the red trajectory is pushed into the singlet region (mid and bottom diagrams). Experimentally, this results in the disappearance of the doublet GS loop structure, as shown in the middle and bottom panels of the first column. The second and third columns show the *B* evolution of the Andreev levels in the three coupling regimes. For relatively weak coupling (top row), the Andreev levels for a singlet GS split because of the Zeeman effect, whereas those for a doublet GS simply move apart. At intermediate coupling (middle row), *B* induces a QPT from a singlet to a spin-polarized GS, as denoted by the appearance of a loop structure (middle row, third panel). At the largest coupling (bottom row), the Zeeman splitting of the Andreev levels is clearly visible over all the V_{pg} range. The splitting is gate dependent with a maximum in the central region.

bottom row, Zeeman-split Andreev levels can be seen all over the spanned V_{pg} range. At $B_x = 0.4$ T (third panel), the inner levels overlap at the Fermi level, which indicates a degeneracy between the $|\uparrow\rangle$ and $|S\rangle$ states. The full phenomenology explained above is reproduced qualitatively by a self-consistent Hartree–Fock treatment of a N–QD–S Anderson model (see Supplementary Information), which thus supports our interpretation in terms of spin-resolved Andreev levels and a QPT.

Interestingly, the splitting of Andreev levels appears to be gate dependent. It tends to vanish when the system is pushed deep into the singlet GS, and it is maximal near the phase boundaries. To further investigate this behaviour, we measured dI/d$V(B,V)$ for fixed values of V_{pg}. These measurements were carried out on a second similar device (see Supplementary Information). The right panel of Fig. 3b displays the B_x dependence of the subgap resonances measured at position 1 in Fig. 3a. Initially, the energy of the Andreev levels increases, as expected for a doublet GS (Fig. 3b, left panel). From a linear fit of the low-field regime, that is $\zeta(B_x) = \zeta(0) + E_Z/2$, where $E_Z = |g_x|\mu_B B_x$ is the Zeeman energy and μ_B is the Bohr magneton, we obtain a *g*-factor $|g_x| \approx 5.6$. For $B_x > 0.7$ T, the field-induced closing of the gap bends the Andreev levels down to zero energy. Finally, above the critical field, a split Kondo resonance is observed, from which $|g_x| \approx 5.5$ is estimated, consistent with the value extracted from the Andreev level evolution. The right panel of Fig. 3c displays a similar measurement taken at position 2 in Fig. 3a, where the GS is a singlet. The splitting of the Andreev levels is clearly asymmetric. The lower level decreases to zero according to a linear dependence, $\zeta_\uparrow(B_x) = \zeta(0) - E_Z/2$, with $|g_x| \approx 6.1$, which is close to the value measured in the normal state. The higher energy level, however, exhibits a much weaker field dependence. Both the nonlinear field dependence for $B_x > 0.7$ T in Fig. 3b and the asymmetric splitting in Fig. 3c can be explained in terms of a level-repulsion effect between the Andreev levels and the continuum of quasiparticle states. This interpretation is corroborated by numerical and analytical modelling, as discussed in the Supplementary Information. In the right panel of Fig. 3c, the inner subgap resonances cross around 1.5 T, which denotes a field-induced QPT where the GS fermion parity changes from even to odd. Above this field, however, they remain pinned as a zero-bias peak (ZBP) up to $B_c^x \approx 2$ T. This peculiar behaviour can be attributed to the level-repulsion effect discussed above, in combination with the rapid shrinking of Δ with B_x.

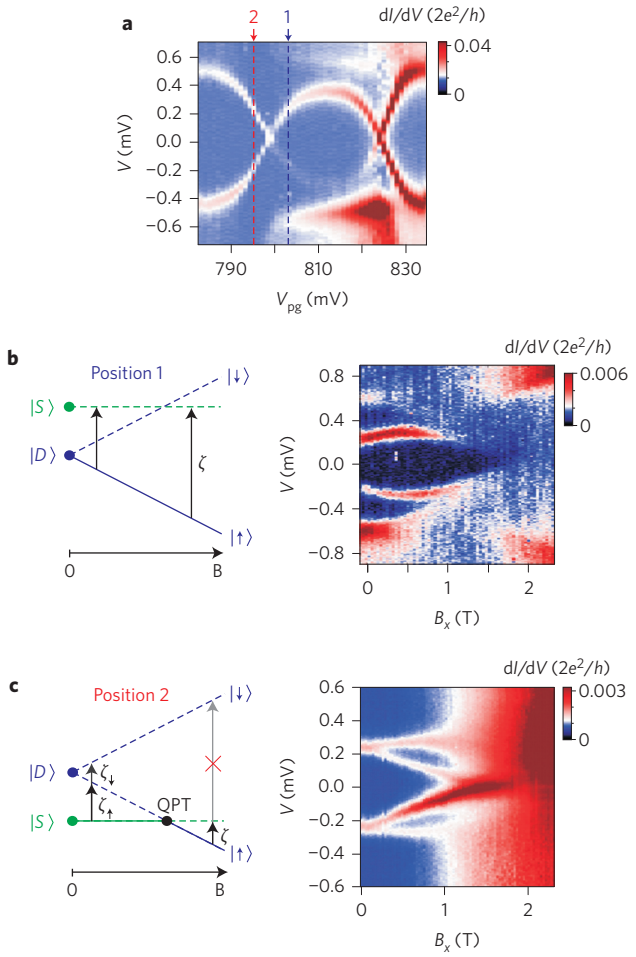

Figure 3 | Magnetic-field evolution of the Andreev levels at fixed gate voltage and the level-repulsion effect. a, $dI/dV(V_{pg},V)$ measurement at $B = 0$ corresponding to a singlet–doublet–singlet sweep. **b**, The left panel shows the qualitative B evolution of the low-energy states of a QD–S system as expected for a doublet GS. The corresponding experimental data measured at position 1 in **a** are shown on the right. ζ increases linearly with B until it approaches the edge of the superconducting gap. The levels then move towards zero following the B suppression of Δ. **c**, Same as **b**, but for a singlet GS. The experimental plot in the right panel was taken at position 2 in **a**. It shows an asymmetric splitting of the $\zeta_\uparrow$ and $\zeta_\downarrow$ peaks. The weak B dependence of $\zeta_\downarrow$ results from the level repulsion between $|\downarrow\rangle$ and the continuum of quasiparticle states above Δ.

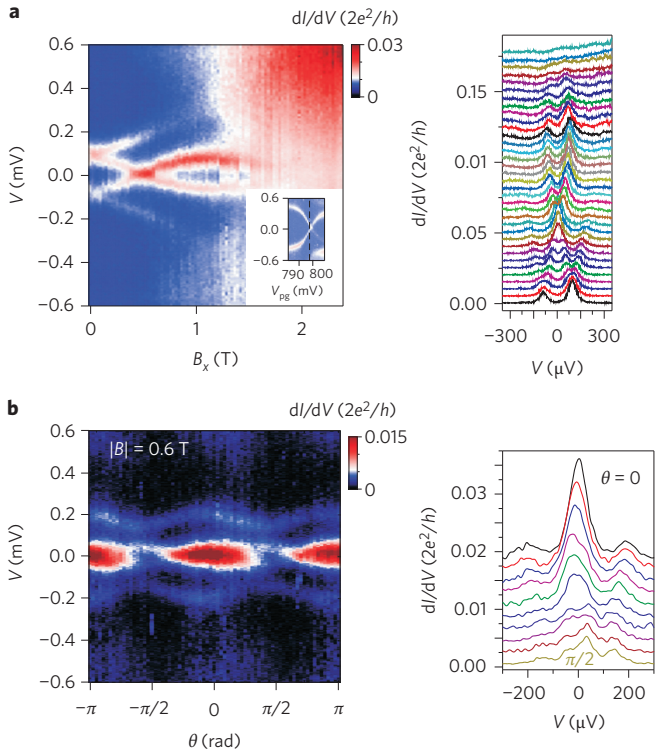

Figure 4 | Magnetic-field induced QPT and angle anisotropy. a, The left panel shows $dI/dV(B,V)$ taken at the position of the vertical line in the inset (same device as in Fig. 3). The right panel shows line traces at equally spaced B values as extracted from the data in the left panel (each shifted by $0.005 \times 2e^2/h$). The QPT induced by the field is observed as a ZBP that extends over a B range of about 150 mT. This apparently large extension is a consequence of the finite width of the Andreev levels. **b**, $dI/dV(V)$ traces taken with $|B| = 0.6$ T, at different angles. This field magnitude corresponds to the QPT field when B is aligned to the NW axis at $\theta = 0$. Owing to the g-factor anisotropy, the ZBP associated with the QPT is split and suppressed when B is rotated away from the NW axis. The peak splitting has a maximum at $\theta = \pi/2$.

To observe a clear B-induced QPT from a singlet to a spin-polarized GS, we reduced $\zeta(0)$ by tuning V_{pg} closer to the singlet–doublet crossing in Fig. 3a. The corresponding data are shown in Fig. 4a. Contrary to the case of Fig. 3c, the Andreev level splitting is rather symmetric, owing to the reduced importance of the level-repulsion effect at energies far from Δ. The inner subgap resonances split again after the QPT, which occurs now at $B_x \approx 0.5$ T. As expected, the outer subgap resonances are abruptly suppressed above this QPT field (Fig. 3c, left panel). The suppression is not complete though, which suggests a partial population of the $|S\rangle$ ES, possibly favoured by thermal activation.

The ZBP at the QPT appear to extend on a sizable field range $\Delta B_x \approx 150$ mT. This range is consistent with the Γ_N-dominated lifetime broadening of the Andreev levels, that is $|g_x|\mu_B \Delta B_x \approx$ peak width ≈ 50 μeV. In Fig. 4b we show how the ZBP depends on the in-plane B angle, θ, relative to the NW axis. As θ varies from 0 to $\pi/2$, the ZBP splits into two peaks with smaller height. This angle dependence is an effect of the g-factor anisotropy. For $\theta = \pi/2$, we find a g-factor $|g_y| \approx 3$, that is a factor of two smaller than for $\theta = 0$ (see Supplementary Information). As a result, the QPT only occurs at a higher field ($B^y_{QPT} \approx 1$ T, see Supplementary Information), and the split peaks correspond to $\zeta_\uparrow$ transitions on the singlet-GS side. Figure 4b also shows a pair of small outer peaks associated with the $\zeta_\downarrow$ transitions. Their oscillatory position is also because of g-factor anisotropy.

The B dependences discussed above mimic some of the signatures expected for Majorana fermions in hybrid devices[7,8,35–43]. A ZBP extending over a sizable B range is observed for $\theta = 0$, and it is suppressed for $\theta = \pi/2$, that is when B is presumably aligned to the Rashba spin-orbit field, B_{SO} (refs 39,40). Although in Fig. 4 the field extension of the ZBP is limited by the ratio between the Andreev-level linewidth and the g-factor, Fig. 3c shows a ZBP extending over a much larger B range. This stretching effect is linked to the field-induced suppression of Δ and the consequently enhanced level repulsion with the continuum of quasiparticle states. In larger QDs or extended NWs, a similar level-repulsion effect may also arise from other Andreev levels present inside the gap[35,36,38,44].

A more detailed discussion of the relation between the results of this work and existing experiments on Majorana fermions is given in Supplementary Section VII. Interestingly, a recent study has shown that zero-energy crossings of Andreev levels associated with a change in the GS parity, similar to those presented here,

adiabatically evolve towards zero energy Majorana modes on increasing the NW length to the infinite-length limit[44]. This evolution might be investigated experimentally in semiconductor–NW systems by studying the B evolution of Andreev levels in NWs of increasing length. Along similar lines, recent proposals discuss the possibility of a gedanken experiment to investigate the short-to-long wire evolution in chains of magnetic impurities deposited on superconducting surfaces[45–49]. In such proposals, the Yu–Shiba–Rusinov bound states induced by the individual magnetic impurities (similar to the Andreev levels discussed here) evolve towards a band when the length of the chain increases and may ultimately lead to Majorana modes localized at the edges of the atom chain.

Methods

Device fabrication. The N–QD–S devices used in this study were based on individual InAs/InP core/shell NWs grown by thermal evaporation[50] (diameter ~30 nm, shell thickness ~2 nm). The NWs were deposited onto Si/SiO_2 substrates on which arrays of thin metallic striplines (Ti (2.5 nm)/Au (15 nm), width ~50 nm) covered by a 8 nm thick atomic layer deposition HfO_2 film had been processed previously. During the measurements, the degenerately doped Si substrate was used as a global backgate, whereas the striplines were used as local gates. Normal metal (Ti (2.5 nm)/Au (50 nm)) and superconductor (Ti (2.5 nm)/V (45 nm)/Al (5 nm)) leads were incorporated into the devices by means of standard e-beam lithography techniques (lateral separation ~200 nm).

Received 17 May 2013; accepted 11 November 2013; published online 15 December 2013

References

1. De Franceschi, S., Kouwenhoven, L. P., Schönenberger, C. & Wernsdorfer, W. Hybrid superconductor–quantum dot devices. *Nature Nanotechnol.* **5,** 703–711 (2010).
2. Hofstetter, L., Csonka, S., Nygård, J. & Schönenberger, C. Cooper pair splitter realized in a two-quantum-dot Y-junction. *Nature* **461,** 960–963 (2009).
3. Herrmann, L. G. *et al.* Carbon nanotubes as Cooper pair splitters. *Phys. Rev. Lett.* **104,** 026801 (2010).
4. Das, A. *et al.* High-efficiency Cooper pair splitting demonstrated by two-particle conductance resonance and positive noise cross-correlation. *Nature Commun.* **3,** 1165 (2012).
5. Cleuziou, J., Wernsdorfer, W., Bouchiat, V., Ondarcuhu, T. & Monthioux, M. Carbon nanotube superconducting quantum interference device. *Nature Nanotechnol.* **1,** 53–59 (2006).
6. Sau, J. D., Lutchyn, R. M., Tewari, S. & Sarma, S. D. Generic new platform for topological quantum computation using semiconductor heterostructures. *Phys. Rev. Lett.* **104,** 040502 (2010).
7. Lutchyn, R. M., Sau, J. D. & Sarma, S. D. Majorana fermions and a topological phase transition in a semiconductor–superconductor. *Phys. Rev. Lett.* **105,** 077001 (2010).
8. Oreg, Y., Refael, G. & von Oppen, F. Helical liquids and Majorana bound states in quantum wires. *Phys. Rev. Lett.* **105,** 177002 (2010).
9. van Dam, J. A., Nazarov, Y. V., Bakkers, E. P. A. M., De Franceschi, S. & Kouwenhoven, L. P. Supercurrent reversal in quantum dots. *Nature* **442,** 667–670 (2006).
10. Buitelaar, M. R., Nussbaumer, T. & Schönenberger, C. Quantum dot in the Kondo regime coupled to superconductors. *Phys. Rev. Lett.* **89,** 256801 (2002).
11. Jorgensen, H. I., Novotny, T., Grove-Rasmussen, K., Flensberg, K. & Lindelof, P. E. Critical current $0–\pi$ transition in designed Josephson quantum dot junctions. *Nano Lett.* **7,** 2441–2445 (2007).
12. Maurand, R. *et al.* First-order $0–\pi$ quantum phase transition in the Kondo regime of a superconducting carbon nanotube quantum dot. *Phys. Rev. X* **2,** 011009 (2012).
13. Doh, Y. J., De Franceschi, S., Bakkers, E. P. A. M. & Kouwenhoven, L. P. Andreev reflection versus Coulomb blockade in hybrid semiconductor nanowire devices. *Nano Lett.* **8,** 4098–4102 (2008).
14. Yamada, Y., Tanaka, Y. & Kawakami, N. Interplay of Kondo and superconducting correlations in the nonequilibrium Andreev transport through a quantum dot. *Phys. Rev. B* **84,** 075484 (2011).
15. Glazman, L. I. & Matveev, K. Resonant Josephson current through Kondo impurities in a tunnel barrier. *JETP Lett.* **49,** 659 (1989).
16. Rozhkov, A. V. & Arovas, D. P. Josephson coupling through a magnetic impurity. *Phys. Rev. Lett.* **82,** 2788–2791 (1999).
17. Vecino, E., Martín-Rodero, A. & Yeyati, A. L. Josephson current through a correlated quantum level: Andreev states and π junction behavior. *Phys. Rev. B* **68,** 035105 (2003).
18. Oguri, A., Tanaka, Y. & Hewson, A. C. Quantum phase transition in a minimal model for the Kondo effect in a Josephson junction. *J. Phys. Soc. Jpn* **73,** 2494–2504 (2004).
19. Bauer, J., Oguri, A. & Hewson, A. C. Spectral properties of locally correlated electrons in a Bardeen–Cooper–Schrieffer superconductor. *J. Phys. Condens. Matter* **19,** 486211 (2007).
20. Choi, M. S., Lee, M., Kang, K. & Belzig, W. Kondo effect and Josephson current through a quantum dot between two superconductors. *Phys. Rev. B* **70,** 020502(R) (2004).
21. Meng, T., Florens, S. & Simon, P. Self-consistent description of Andreev bound states in Josephson quantum dot devices. *Phys. Rev. B* **79,** 224521 (2009).
22. Domański, T., Donabidowicz, A. & Wysokiński, K. I. Meservey–Tedrow–Fulde effect in a quantum dot embedded between metallic and superconducting electrodes. *Phys. Rev. B* **78,** 144515 (2008).
23. Futterer, D., Swieboddzinski, J., Governale, M. & König, J. Renormalization effects in interacting quantum dots coupled to superconducting leads. *Phys. Rev. B* **87,** 014509 (2013).
24. Kanai, Y. *et al.* Electrical control of Kondo effect and superconducting transport in a side-gated InAs quantum dot Josephson junction. *Phys. Rev. B* **82,** 054512 (2010).
25. Sand-Jespersen, T. *et al.* Kondo-enhanced Andreev tunneling in InAs nanowire quantum dots. *Phys. Rev. Lett.* **99,** 126603 (2007).
26. Eichler, A. *et al.* Even–odd effect in Andreev transport through a carbon nanotube quantum dot. *Phys. Rev. Lett.* **99,** 126602 (2007).
27. Pillet, J. D. *et al.* Andreev bound states in supercurrent-carrying carbon nanotubes revealed. *Nature Phys.* **6,** 965–969 (2010).
28. Deacon, R. S. *et al.* Tunneling spectroscopy of Andreev energy levels in a quantum dot coupled to a superconductor. *Phys. Rev. Lett.* **104,** 076805 (2010).
29. Dirks, T. *et al.* Transport through Andreev bound states in a graphene quantum dot. *Nature Phys.* **7,** 386–390 (2011).
30. Lee, E. J. H. *et al.* Zero-bias anomaly in a nanowire quantum dot coupled to superconductors. *Phys. Rev. Lett.* **109,** 186802 (2012).
31. Chang, W., Manucharyan, V. E., Jespersen, T. S., Nygåard, J. & Marcus, C. M. Tunneling spectroscopy of quasiparticle bound states in a spinful Josephson junction. *Phys. Rev. Lett.* **110,** 217005 (2013).
32. Pillet, J. D., Joyez, P., Zitko, R. & Goffman, M. F. Tunneling spectroscopy of a single quantum dot coupled to a superconductor: from Kondo ridge to Andreev bound states. *Phys. Rev. B* **88,** 045101 (2013).
33. Kumar, A. *et al.* Temperature dependence of Andreev spectra in a superconducting carbon nanotube quantum dot. Preprint at http://lanl.arXiv.org/1308.1020v1 (2013).
34. Giazotto, F. *et al.* A Josephson quantum electron pump. *Nature Phys.* **7,** 857–861 (2011).
35. Prada, E., San-Jose, P. & Aguado, R. Transport spectroscopy of N–S nanowire junctions with Majorana fermions. *Phys. Rev. B* **86,** 180503(R) (2012).
36. Rainis, D., Klinovaja, J. & Loss, D. Towards a realistic transport modeling in a superconducting nanowire with Majorana fermions. *Phys. Rev. B* **87,** 024515 (2013).
37. Sarma, S. D., Sau, J. D. & Stanescu, T. D. Splitting of the zero-bias conductance peak as smoking gun evidence for the existence of the Majorana mode in a superconductor–semiconductor nanowire. *Phys. Rev. B* **86,** 220506(R) (2012).
38. Liu, J., Potter, A. C., Law, K. T. & Lee, P. A. Zero-bias peaks in the tunneling conductance of spin-orbit-coupled superconducting wires with and without Majorana end-states. *Phys. Rev. Lett.* **109,** 267002 (2012).
39. Mourik, V. *et al.* Signatures of Majorana fermions in hybrid superconductor–semiconductor nanowire devices. *Science* **336,** 1003–1007 (2012).
40. Das, A. *et al.* Zero-bias peaks and splitting in an Al–InAs nanowire topological superconductor as a signature of Majorana fermions. *Nature Phys.* **8,** 887–895 (2012).
41. Deng, M. T. *et al.* Anomalous zero-bias conductance peak in a Nb–InSb nanowire–Nb hybrid device. *Nano Lett.* **12,** 6414–6419 (2012).
42. Finck, A. D. K., van Harlingen, D. J., Mohseni, P. K., Jung, K. & Li, X. Anomalous modulation of a zero-bias peak in a hybrid nanowire-superconductor device. *Phys. Rev. Lett.* **110,** 126406 (2012).
43. Churchill, H. O. H. *et al.* Superconductor-nanowire devices from tunnelling to multi-channel regime: zero-bias oscillations and magnetoconductance crossover. *Phys. Rev. B* **87,** 242401(R) (2013).
44. Stanescu, T. D., Lutchyn, R. M. & Sarma, S. D. Dimensional crossover in spin-orbit-coupled semiconductor nanowires with induced superconducting pairing. *Phys. Rev. B* **87,** 094518 (2013).
45. Nadj-Perge, S., Drozdov, I. K., Bernevig, B. A. & Yazdani, A. Proposal for realizing Majorana fermions in chains of magnetic atoms on a superconductor. *Phys. Rev. B* **88,** 020407(R) (2013).
46. Klinovaja, J., Stano, P., Yazdani, A. & Loss, D. Topological superconductivity and Majorana fermions in RKKY systems. *Phys. Rev. Lett.* **111,** 186805 (2013).
47. Vazifeh, M. M. & Franz, M. Self-organized topological state with Majorana fermions. *Phys. Rev. Lett.* **111,** 206802 (2013).

48. Braunecker, B. & Simon, P. Interplay between classical magnetic moments and superconductivity in quantum one-dimensional conductors: towards a self-sustained topological Majorana phase. *Phys. Rev. Lett.* **111,** 147202 (2013).
49. Pientka, F., Glazman, L. & von Oppen, F. Topological superconducting phase in helical Shiba chains. *Phys. Rev. B* **88,** 155420 (2013).
50. Jiang, X., Xiong, Q., Qian, F., Li, Y. & Lieber, C. M. InAs/InP radial nanowire heterostructures as high electron mobility devices. *Nano Lett.* **7,** 3214–3218 (2007).

Acknowledgements

This work was supported by the European Research Council (ERC Grant agreement no. 280043-HybridNano) and by the Agence Nationale de la Recherche (ANR-08-JCJC-0010). R.A. acknowledges support from the Spanish Ministry of Economy and Innovation through grants FIS2009-08744 and FIS2012-33521. The authors thank J-D. Pillet for useful discussions.

Author contributions

E.J.H.L. and S.D.F. conceived the experiment. X.J. grew the semiconductor NWs under C.M.L.'s supervision. E.J.H.L. fabricated the devices and performed all the measurements under S.D.F.'s supervision. R.A. performed the Hartree–Fock calculations, and M.H. carried out the analytical study of the level-repulsion effect. E.J.H.L., S.D.F., R.A. and M.H. analysed and interpreted the results. All authors co-wrote the manuscript.

Additional information

Supplementary information is available in the online version of the paper. Reprints and permissions information is available online at www.nature.com/reprints. Correspondence and requests for materials should be addressed to S.D.F.

Competing financial interests

The authors declare no competing financial interests.